Bonding and Electronic Consideration in the Metal-Metal Bonded Edge Sharing Complexes

Jaejung Ko* and Kuk-Tae Park

Department of Chemical Education, Korea National University of Education, Choungbuk 363-791

Ikchoon Lee and Bon-Su Lee

Department of Chemistry, Inha University, Incheon 402-751. *Received July 11, 1989*

The molecular interaction of $W_2(NH_2)_4Cl_4$ fragment with chlorine ligands has been studied by means of extended Hückel calculations. We have extended the Hückel calculation to unknown edge-sharing $W_2(NH_2)_4Cl_4(\mu\text{-}X)_2$ complexes (X = CO, H) in order to compare the stability of the complexes. The calculations showed that the size and electronic property of bridged ligand are important in determining the stability. The stabilities of the related metal-metal bonded edge-sharing complexes are discussed.

Introduction

The edge-sharing complexes are well known in transition metal chemistry.[1] They show many striking features because they exhibit a broadly applicable and flexible framework. Therefore, the eximination of the interaction between adjacent metal atoms is intrigued.

Recognition of various factors in the interaction is important in understanding many aspectes of complexes. Among many relevant studies, we would like to point out an elegant work of Cotton[2] reported on the structure of metal-metal bonded edge-sharing bioctahedral complexes. The ground-state electronic structures of the model compound $Ta_2Cl_4(PH_3)_4H_2$ was reported by Sattelberger and coworkers[3] using the multiple-scattering X_α method. Recently, we[4] have studied the bonding and electronic considerations in the apex bridged $M_2(OR)_6L(\mu\text{-}X)$ complexes (M = Mo; R = -t-Bu, -i-Pr; L = Py; $x = o$ or 2; X = CO, SO_2, HCCH, H, and Cl). Since we are interested in the electronic structure and bonding of various bridging ligands ranging from single atom bridges such as Cl, H, and S to small molecule such a HC-CHCHCH, we decided to investigate the bonding in the complexes of the general type $M_2X_4Y_2Z_4$ [M = Mo, W, Ta; X = SH, NH_2, Cl, OH; Y = Cl, H, S, CO, C_4H_4 (the ferrole); Z = OH, Cl, NH_2] such as edge-sharing bioctahedron of type 1 and ferrole complex of type 2.

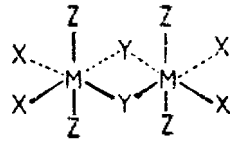

1

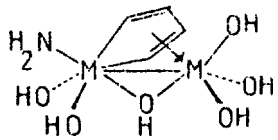

2

As a first step, the molecular orbitals were constructed for the $M_2X_4Z_4$ fragment, and then their interactions with each different bridged ligand were computed.

All calculations are of the extended Hückel type, and the parameter used are tabulated in Appendix I.

Single-Atom Bridged Edge-Sharing Complexes. There are many small-molecule bridged edge-sharing complexes for which crystal structures are available. Among them, we chose the chlorine bridged $W_2(Py)_4Cl_4(\mu\text{-}Cl)_2$[5] (3), carbonyl bridged $W_2(NH_2)_4Cl_4(\mu\text{-}CO)_2$ (4), sulfur bridged $W_2(OMe)_4(S_2CNEt_2)_2(\mu\text{-}S)_2$[6] (5) and hydrogen bridged $Ta_2(PMe_3)_4Cl_4(\mu\text{-}H)_2$ (see below) in order to see the stability dependence of the complexes on the size of bridging ligand, π-donor, acceptor ligands, and terminal ligands.

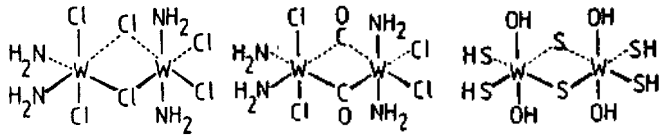

3 4 5

In this section, we discuss the bonding and electronic structure of μ-Cl and μ-CO bridged edge-sharing complexes. Afterward, we will extend the general bonding features studied in both complexes to the $(\mu\text{-}OH)_2$ and $(\mu\text{-}Br)_2$ complexes. As a first step, we replaced the methyl group on the phosphine by hydrogen and ethylthiocyanide ligand by SH_2 group in order to simplify the calculations; pyridine was replaced by NH_2 group. Let us start from the orbitals of $W_2(NH_2)_4Cl_4$. They are derived from those of $W(NH_2)_2Cl_2$ fragment with a C_{2v} point group for each tungsten atom. The important metal-based molecular orbitals are shown on the left side in Figure 1. The geometry of $W_2(NH_2)_4Cl_4$ can be thought of as a combination of two octahedral fragments with two chlorines shared. In the valence orbitals of $W_2(NH_2)_4Cl_4$ fragement, at high energy side is a primarily metal yz orbital of $2a_2$ followed by $1b_2$. The $1b_2$ orbital consists of a mixture of xy and x character. The $1a_2$ orbital consists mainly of metal yz character. At low energy side are the $1b_1$ and $3a_1$ orbitals of predominatly metal xz and $x^2\text{-}y^2$, respectively. In the molecular orbitals, a question may be raised as to why the $2a_2$ metal-metal orbital of an antibonding character gives a slight difference in energy (0.41eV) compared with $1a_2$ orbital in a bonding fashion. A slight difference may be attributable to the poor overlap between the two metal atoms which are located apart (2.73Å) and the bonding interaction between the metal $2a_2$ orbital and hybrids of the surrounding ligands. The $1a_2$ and $2a_2$ orbitals with the interaction between the metal d orbitals and π hybrids of the ligands are shown schematically in 6 and 7, respectively.

As shown above, a set of two chlorine ligands have an π^*-bonding interaction with the yz orbital of $1a_2$ orbital. On

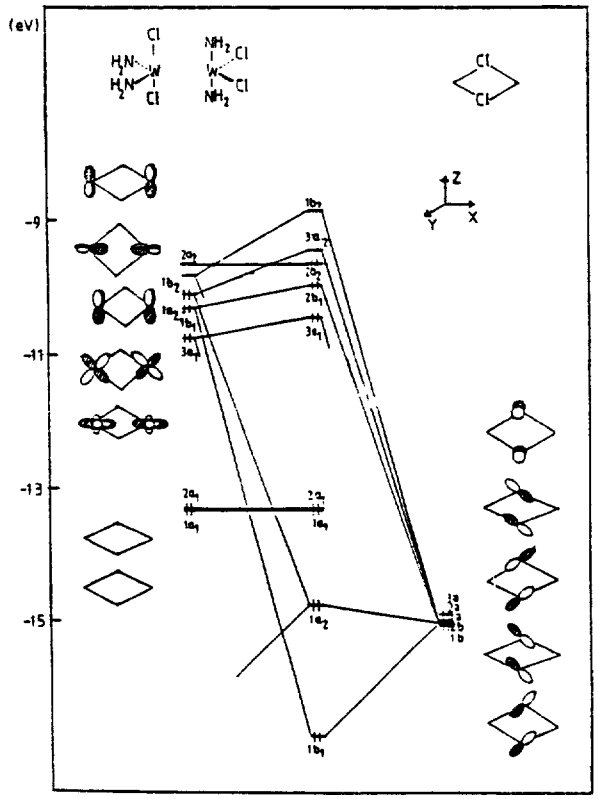

Figure 1. Correlation diagram of orbitals for $W_2(NH_2)_4Cl_4(\mu\text{-}Cl)_2$ with $W_2(NH_2)_4Cl_4$ and Cl_2.

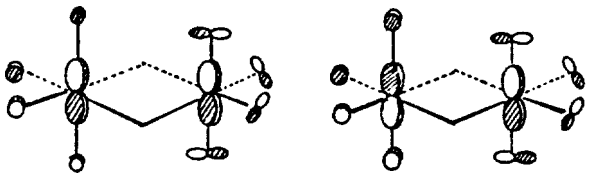

6 7

the other hand, the corresponding two chlorine ligands interacts with the *yz* orbital in a bonding fashion to produce Mo-Cl π bond in the $2a_2$ orbital. These results explain why the metal-metal bonding $1a_2$ orbital has a relatively small energy gap compared with that of $2a_2$ orbital. This pattern is similar to that of apex bridged $M_2(OR)_6(\mu\text{-}X)$ complexes[4] in which the metal-metal bonding $3a_1$ orbital is more destabilized than the metal-metal anti-bonding $1b_2$ orbital due to the strong interaction between metal d orbital and alkoxide σ and π hybrids rather than the interaction of metal-metal bond. Let us turn to the problem of specifying the electron count around the metal in order to evaluate the metal-metal bond. If we count a bridging chlorine as negative Cl^{-1}, the oxidation state of Mo(V) gives a dimetal fragment, which gives a d^1-d^1 single bond length. The distance of metal-metal bond (2.73Å) in the known complex $W_2(py)_4Cl(\mu\text{-}Cl)_2$ is indeed comparable. The electornic structure of $W_2(NH_2)_4Cl_4(\mu\text{-}Cl)_2$ is easily constructed by interacting a $W_2(NH_2)_4Cl_4$ fragement with $(\mu\text{-}Cl)_2$ fragment. Figure 1 shows an orbital interaction diagram for $W_2(NH_2)_4Cl_4(\mu\text{-}Cl)_2$. Before combining a symmetry adapted linear combination, let us review the frontier orbitals of chlorine. The chlorine has a relatively high P_y orbital and five low energy orbitals consisting of a mixture of P_x and P_z orbitals. On the center of this Figure, the atomic

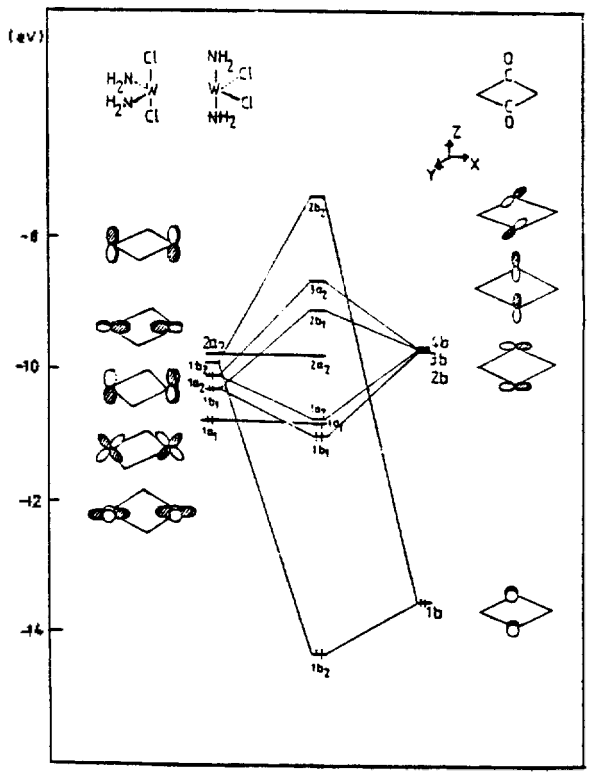

Figure 2. Correlation diagram of orbitals for $W_2(NH_2)_4Cl_4(\mu\text{-}CO_2)$ with $W_2(NH_2)_4Cl_4$ and $(\mu\text{-}CO)_2$.

(P_x+P_y) orbital (1b) on chlorine interacts with the $1b_1$ metal-metal bonded fragment orbital in a bonding fashion to produce a W-Cl π bonded molecular orbital, labelled as 1b, and an antibonding counterpart, $2b_1$, which is predominantly of the metal $1b_1$ orbital. At high energy side, the 1b and 2b orbitals of chlorines interact with the $1b_1$ and $1b_2$ of metals in an antibonding fashion to produce a W-Cl π^* bond. The $1a_2$ composite orbital on the center is formed by three orbital interactions with the $1a_2$, another lower a_2 orbital of $W_2(NH_2)_4Cl_4$ fragment and 1a orbital of Cl_2 fragment. The $2a_2$ orbital is essentially nonbonding as the HOMO. The $3a_2$ orbital is mainly the *yz* metal-metal molecular orbital as the LUMO. Since there is a relatively small gap (0.28 eV) in energy between the HOMO and LUMO, a second order Jahn-Tellar distortion between $2a_2$ and $3a_2$ is expected due to the same symmetry of HOMO($2a_2$) and LUMO($3a_2$). Consideration of the distortion should lead to a large energy gap than that of a calculated value. Therefore, it is not surprising that related Cl bridged edge-sharing complexes such as $Ta_2(PMe_3)_4Cl_4(\mu\text{-}Cl)_2$[7], $Mo_2(DPPM)_2Cl_4(\mu\text{-}Cl)_2$[9] have been prepared. In the isolobal complex $W_2(NH_2)_4Cl_4(\mu\text{-}OH)_2$, the calculations show a relatively large energy gap (1.59eV) between the HOMO($2a_2$) and LUMO($3a_2$). It is well documented that μ-OH bridge edge-sharing complexes such as $W_2(OEt)_2(HOEt)_2Cl_4(\mu\text{-}OEt)_2$[10], $W_2(OCHEt_2)_2(HOCHEt_2)_2Cl_4(\mu\text{-}OEt)_2$[11], and $W_2(OMe)_2(MeOH)_2Cl_4(\mu\text{-}OMe)_2$[10] have been prepared.

Now let us turn to the CO bridged edge sharing complex in order to compare the stability of π-acceptor ligand with π-donor ligand. Crystal structure of $W_2(NH_2)_4Cl_4(\mu\text{-}CO)_2$ complex is not known, although related $W_2(OPr)_6(\mu\text{-}CO)_2$[12] and $Pt(\mu\text{-}CO)Cl_2(dam)$[13] complexes have been prepared. It is well known that the role of bridged CO ligand is quite dif-

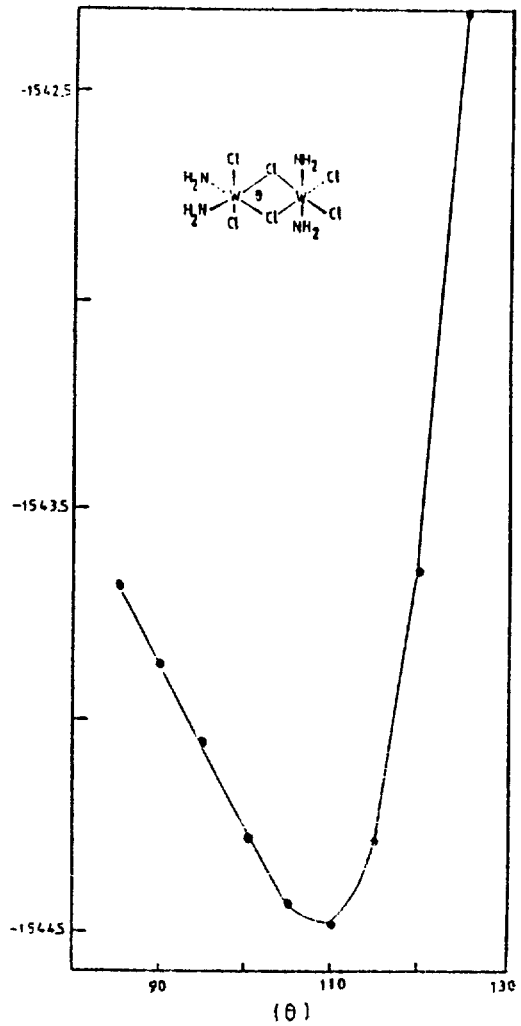

Figure 3. Potential curve of $W_2(NH_2)_4Cl_2(\mu\text{-}Cl)_2$ as a function of angle.

ferent from that of Cl ligand because the CO ligand is π-acceptor and the Cl ligand π-donor. In the treatment of $W_2(NH_2)_4Cl_4(\mu\text{-}CO)_2$ complex, we counted the bridged carbonyl as dinegative CO^{2-}.[14] In that case, the metal-metal fragment has a $d^\circ - d^\circ$ configuration. Indeed, if we assume the distance between two metal is 2.73Å, which is a single bond distance, the gap in energy between the HOMO and LUMO is 0.08eV. It led to a paramagnetic complex. On the other hand, when we take the distance as 3.20Å, the gap becomes bigger. The compound becomes stable energetically. In order to see the effect of the π acceptor ligand. We now turn to the interaction diagram. Figure 2 is the interaction diagram for $W_2(NH_2)_4Cl_4(\mu\text{-}CO)_2$. On the left side of this figure are the important valence orbitals of the $W_2(NH_2)_4Cl_4$ fragment. On the right side of this figure are the valence orbitals of CO^{2-} fragment. The filled 1b orbital of CO^{2-} interacts strongly with the $2b_2$ orbital of $W_2(NH_2)_4Cl_4$ to produce π and π^* bonds. The unfilled 1a, 2b, and 3b orbitals of CO^{2-} mix strongly with $1b_1$ and $1a_2$. The HOMO is the $1a_1$, which is predominantly of the metal $x^2\text{-}y^2$ character. Our calculations reveal that the HOMO is actually nonbonding. The $1b_1$ orbital in the $W_2(NH_2)_4Cl_4(\mu\text{-}CO)_2$ complex is primarily of the $1b_1$ metal-metal molecular orbital as the LUMO. Since there is a small gap(0.08eV) in energy between the HOMO

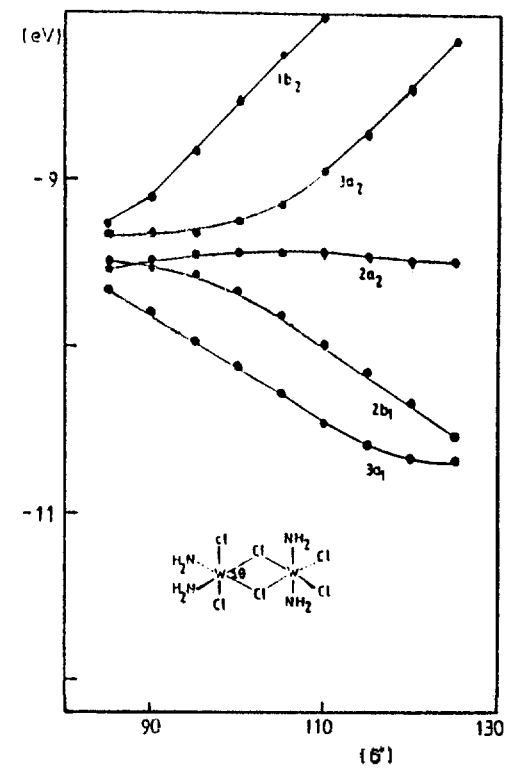

Figure 4. Walsh diagram of $W_2(NH_2)_4Cl_2(\mu\text{-}Cl)_2$ as a function of angle.

and LUMO and poor molecular interaction between $1b_1$ and 2b orbitals, it may be reasonable to predict that the unknown complex $W_2(NH_2)_4Cl_4(\mu\text{-}CO)_2$ can not be prepared.

Now we consider the potential curve and a Walsh diagram as a function of θ with the distance between two metals fixed. Figure 3 shows the potential curve of $W_2(NH_2)_4Cl_4(\mu\text{-}CO)_2$ as function of θ. The geometrical optimization afforded the value of $\theta = 110°$. Figure 4 is a Walsh diagram as a function of θ. It shows us the orbitals which have predominant effects. The most effective orbitals on the stability of the compound are $3a_1$, $2b_1$, and $3a_2$. The $3a_1$, $2b_1$, and $3a_2$ orbitals including the interaction between the metal d orbitals and π hybrids of the ligands are shown schematically in 8-10.

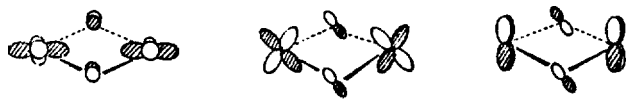

8($3a_1$) 9($2b_1$) 10($3a_2$)

As shown in Figure 4, the $2a_2$ orbital is independent of θ because the $2a_2$ orbital is essentially nonbonding. The abrupt decrease in energy in the case of $3a_1$ and $2b_1$ orbitals can be easily explained by an increasing good overlap between their orbitals as the angle is increased. On the other hand, the $3a_2$ orbital gives a worse π^* antibonding orbital as the angle is increased. It becomes more unstable. Therefore, the stability of the compound may be attributed to the two orbitals, $3a_1$ and $2b_1$.

In an analogous fashion with chlorine bridged $W_2(NH_2)_4Cl_4(\mu\text{-}Cl)_2$ compound, the sulfur atoms in $W_2(SH)_4(OH)_4(\mu\text{-}S)_2$ complex are located at the bridged edge-sharing position. The central W_2S_2 unit is very similar to those commonly

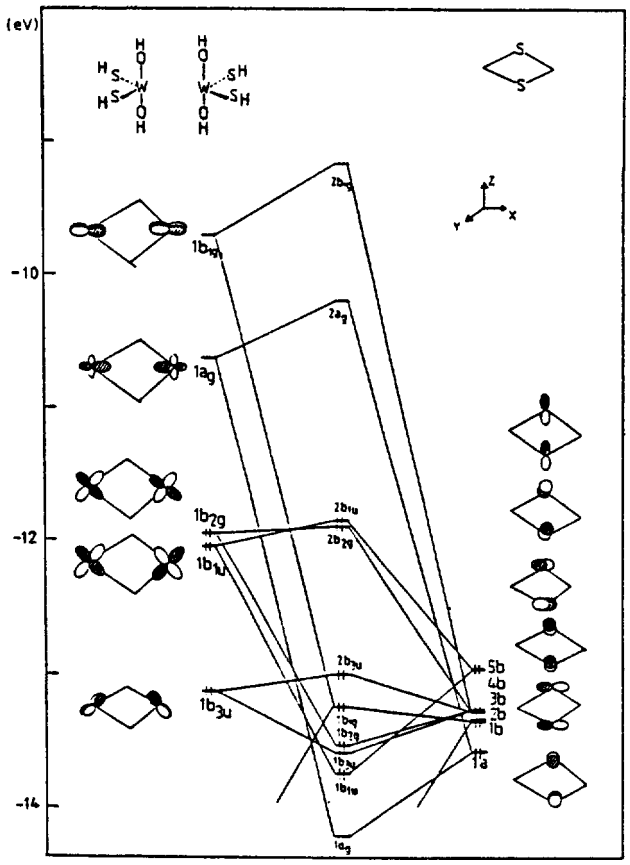

Figure 5. Interaction diagram for $W_2(SH)_4(OH)_4(\mu\text{-}S)_2$.

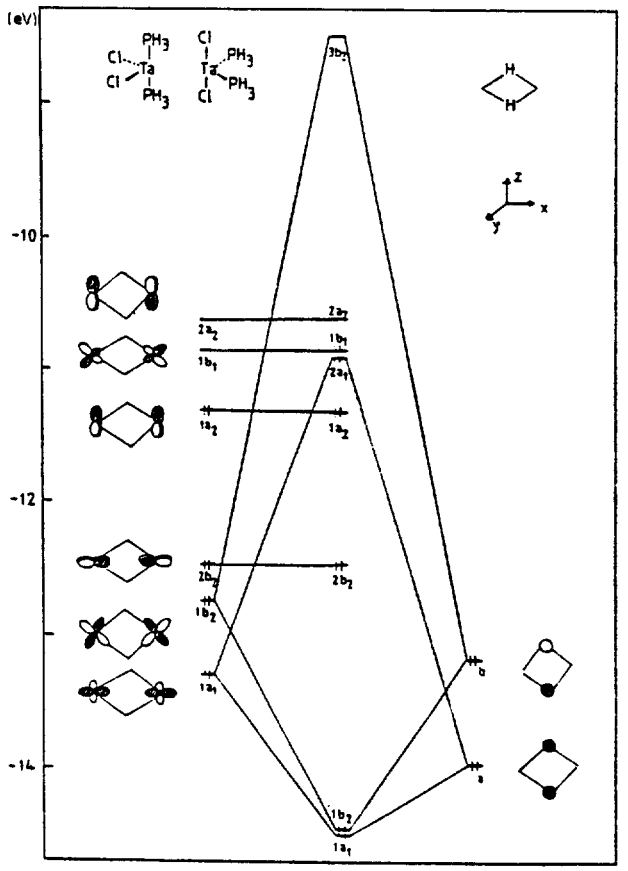

Figure 6. Interaction diagram for $Ta_2(PH_3)_4Cl_4(\mu\text{-}H)_2$.

found in dinuclear organometallic complexes such as $Nb_2(CH_3CN)_4Cl_4(\mu\text{-}S)_2$[15], $W_2(OMe)_4(S_2CNEt_2)_4(\mu\text{-}S)_2$[6], and $Nb_2(SC_4H_8)Cl_4(\mu\text{-}S)_2$. We chose this compound in order to compare the effect of size, electronegativity, and the influence of terminal ligands with those of $W_2(NH_2)_4Cl_4(\mu\text{-}Cl)_2$. Our calculations reveral $W_2(NH_2)_4Cl_4(\mu\text{-}S)_2$ to be stable electronically and energetically. Figure 5 shows an orbital interaction diagram for $W_2(SH)_4(OH)_4(\mu\text{-}S)_2$. On the left side of the figure are the important valence orbitals of $W_2(SH)_4(OH)_4$ fragment with a D_{2h} symmetry. Let us review the sulfur frontier orbitals. The sulfur ligand has one low y orbital and two low x and a mixture of $(x+y)$ orbitals. At high energy side are three orbitals of a mixture of $(x+y)$ and z character. In the valence orbitals of $W_2(SH)_4(OH)_4$ fragment, at high energy side is a primarily metal xy orbital of 1 b_{1g} symmetry. The combination of $x^2\text{-}y^2$ and x atomic character gives the a_{1g} fragment orbital. The $1b_{2g}$ and $1b_{1u}$ orbitals consist of the metal-metal xz orbital in an antibonding and bonding fashion, respectively. At low energy side is the $1b_{3u}$ orbital consisting of a mixture of xy and yz. On the center of the Figure, the atomic z orbital on sulfur interacts with $1a_g$ metal-metal bonding fragement orbital in a bonding fashion to produce a σ W-S bonded molecular orbital, labelled as $1a_g$ and an antibonding counterpart $2a_{1g}$. The sulfur x and z orbitals mix into the $1b_{1g}$ and $1b_{1u}$ orbitals on metal site to produce the $1b_{1g}$ and $1b_{1u}$ bonding orbitals, respectively. The $1b_{1g}$ orbital is formed by mixing three orbitals of the two b_{1g} orbitals and 2b orbital. The three important bonding combinations $2b_{2g}$, $2b_{1u}$, and $2a_g$ between metal fragments and sulfur orbitals are represented in 11-13.

The HOMO ($2b_{1u}$ orbital) can be thought of as representing π bond. It was formed from the combination of metal $1b_{1u}$ orbital with sulfur 1a orbital. The molecular $2a_g$ orbital as the LUMO is predominantly of $1a_g$ metal-metal molecular character. There is a relatively large gap (1.62eV) in energy between the HOMO and LUMO. Moreover, the strong interaction of $1b_{1u}$ and $1b_{2g}$ molecular orbitals in a bonding fashion compared with antibonding interactions between their antibonding counterparts may be an important factor in giving stability of the complex. Therefore, the stability of the complex may be attributable to the two effects. One of them is the effect of size in the bridged ligand. Since the distance between two metals is 2.79Å, comparable to that of $W_2(NH_2)_4Cl_2(\mu\text{-}Cl)_2$, small size of sulfur compared with that of chlorine provides good fit for the bridged ligand. Therefore, it gives a good overlap between two fragments because the direction of p orbital is not distorted from d orbital. Another effect comes from the influence of terminal ligands. The low energies of the d orbitals (-9.7~-13.2eV) in $W_2(SH)_4(OH)$ compared with those (-9.5eV~-10.2eV) in $W_2(NH_2)_4Cl_4$ demonstrate the effect. Indeed, it is not surprising that a lot of related μ-S bridged complexes such as $W_2(OMe)_4(S_2\ CNEt_2)_4(\mu\text{-}S)_2$, $Ta_2(SMe_2)_2Cl_6(\mu\text{-}SPh)_2$[17], and $Mo_2(dppm)_2Cl_4(\mu\text{-}SEt)_2$[18] have been prepared.

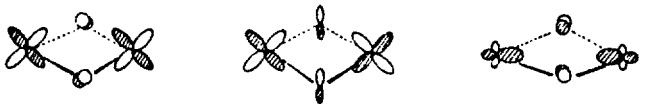

11($2b_{2g}$) 12($2b_{1u}$) 13($2a_g$)

In an analogous fashion to the sulfur bridged $W_2(SH)_4$

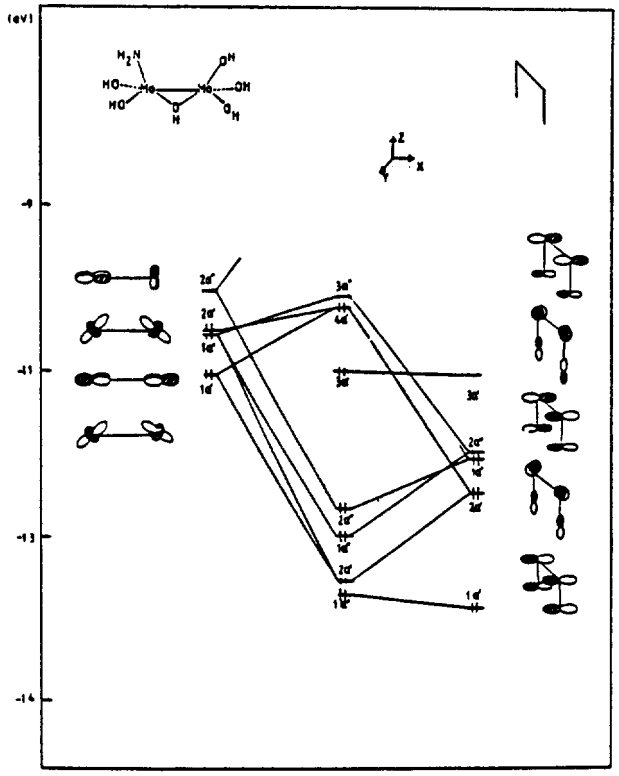

Figure 7. Interaction diagram for $Mo_2(OH)_6(NH_2)(c_4H_4)$.

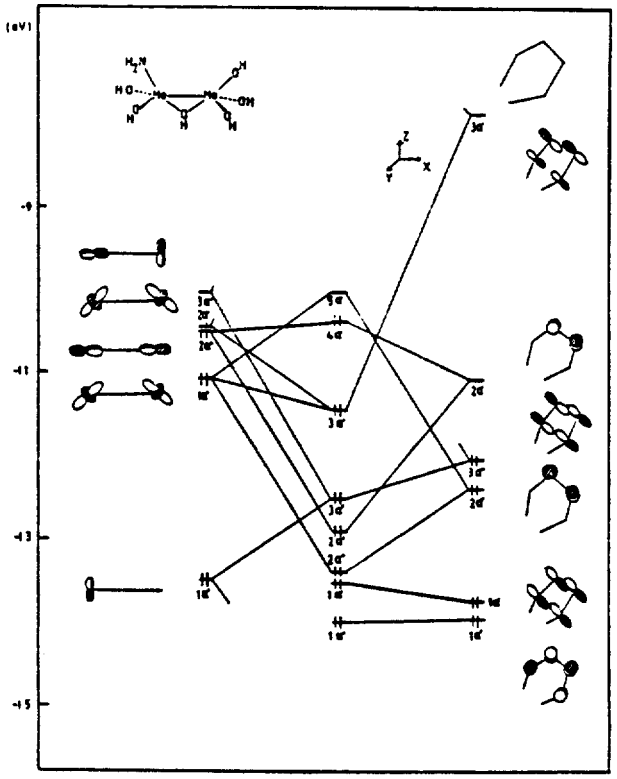

Figure 8. Interaction diagram for the ferrole.

$(OH)_4(\mu\text{-}S)_2$ complex, we chose the hydrogen bridged complex for which the crystal structure is available in order to see a size effect. Our preliminary calculations on $W_2(NH_2)_4Cl_4(\mu\text{-}H)_2$ show that the complex is energetically unstable but, electronically, relatively stable. Then we turn to construct the molecular interaction diagram of a real complex $Ta_2(PMe_3)_4Cl_4(\mu\text{-}H)_2$. Figure 6 shows an ortibal interaction diagram for $Ta_2(PH_3)_4Cl_4(\mu\text{-}H)_2$. On the left side are the important valence orbitals of $Ta_2(PH_3)_4Cl_4$ fragment with a C_{2v} symmetry. At high energy side are $2a_2$ which is of primarily metal *yz* character. The $1b_1$ is a mixture of metal *xz* and *x* character and the $1a_2$ essentially a nonbonding metal *yz* character. At low energy side are $2b_2$ and $1b_2$, a set of predominantly metal *xy* and *xz* character. The lower $1a_1$ orbital consists of mixture of $x^2\text{-}y^2$ and *s* character. In the molecular interaction, the atomic a orbital of hydrogens interacts with the $1a_1$ metal-metal bonding fragment orbital in a bonding fashion to produced a σ Ta-H bonded molecular orbital, $1a_1$, and an σ^* antibonding counterpart, $2a_1$. The hydrogen *b* orbital interacts with the $1b_2$ orbital on metal fragment to produce $1b_2$ σ bonding as the HOMO. The $2a_2$ orbital consists of mainly metal-metal molecular *yz* character as the LUMO. We still have not answered the question as to why the hydrogen bridged complex is unstable. The instability of the complex may result from the $2a_1$ orbital. The $2a_1$ orbital formed by antibonding combination is much higher in energy compared with energy lowering of the $1a_1$ orbital. In spite of the energy gained by the two electrons in the $1b_2$ orbital, the stabilized energy is still small. This may be the reason why the complex is unstable. Indeed, the complex $Ta_2(PMe_3)_4Cl_4(\mu\text{-}H)_2$ is very air sensitive at low temperature, decomposing within seconds on exposure to air.

Small-Molecule Bridged Complex. In this section we extend the bonding of single-atom bridged edge-sharing complexes to that of small molecule bridged complex such as the ferrole in order to examine the effect of orbital interaction by the orbitals of the bridging groups and geometrical preference. Among many known ferrole complexes, several structural determinations are reported. Two examples such as ferrole complex of type 14, and ferrole complex $[Mo_2(OH)_6(NH_2)(C_4H_4)]$[19] containing alkoxide of type 15 are shown below.

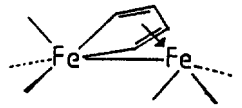

14

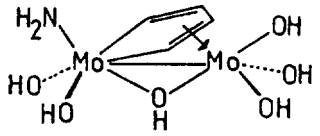

15

As an outstanding example of the relevant previous studies, Hoffmann and coworker[20] reported on the theoretical study of $Fe_2(CO)_6(C_4H_4)$. We attempted a symtematic theoretical analysis of the type 15 involving a single-atom bridged edge-sharing complex. A starting point for an interaction analysis is a hypothetical $Mo_2(OH)_6(NH_2)(C_4H_4)$ structure of C_s symmetry (16).

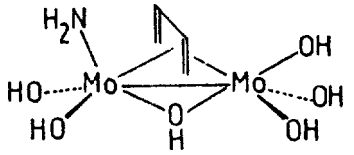

16

The interaction diagram of this geometry is shown in Figure 7. For the electron count around the metal, the fragments are taken as butadienyl dianion and $Mo_2(OH)_6(NH_2)^{2+}$ for the sake of the consistency with other ligands. Figure 8 shows an orbital scheme for a ferrole complex with C_s geometry. The important metal-based molecular orbitals are shown on the left side in Figure 8. In the valence orbitals of the $Mo_2(OH)_6(NH_2)$ fragment, at high energy side is the 2a″ orbital which is primarily of metal *xy* character. The 2a′ and 1a′ orbitals consist of a combination of z^2 and *x* character. The butadienzyl fragment has three π-type orbitals and two σ-type orbitals. In the molecular interaction ten electrons enter this bonding scheme in an analogous fashion to the ferrole $Fe_2(CO)_6(C_4H_4)$ complex. Eight of them are accommodated in bonding orbitals. The highest occupied and low-lying unoccupied orbitals are shown below (17-18).

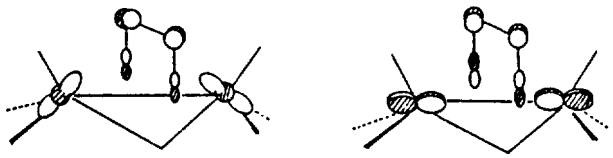

17, HOMO 18, LUMO

In order to compare the stability of $Mo_2(OH)_6(NH_2)(C_4H_4)$ with C_{2s} symmetry[16] with that of the ferrole complex[15] and predict the geometrical preference in both structures, it is intructive to consider the motion of 5a, 6a, and 2b symmetry in 16. The orbital scheme of the ferrole complex $Mo_2(OH)_6(NH_2)C_4H_4$ is shown in Figure 8. The corresponding orbitals are the 3a′, 4a′, and 5a′, as shown in 19-21.

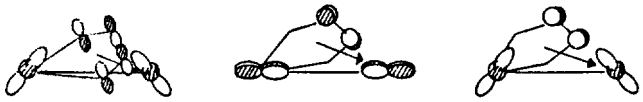

19(3a′) 20(4a′) 21(5a′)

The 3a′ orbital (19) is considerably stabilized due to the increasing overlap between C_2 and C_3 of the butadienyl and *d* orbital compared with the interaction of δ bonding between C_1 and C_4 of the butadienyl and *xy* orbital. In the HOMO orbital (17), increasing overlap leads to a destabilization because they have opposite phases. On the other hand, the HOMO of the ferrole complex has a poor overlap between *p* and *xy* orbital as shown 20. Therefore, the HOMO of compound 15 is stable compared with that of compound 17. The LUMO of structure 16 consists of an effective overlap between C_2 and C_3 of the butadienyl and *d* orbital, leading to a destabilization. An Walsh diagram for three orbitals in both complexes are shown below.

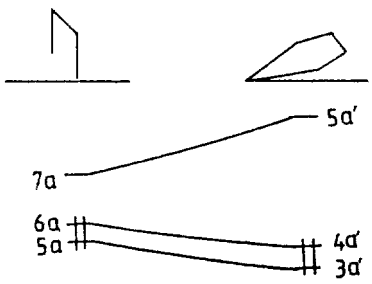

Table 1. Extend Huckel Calculation Parameters

Atom	Orbital	H_{ii}(eV)	ξ_{i1}	$(C_1)^a$	ξ_{i2}	$(C_2)^a$	Ref.
Mo	5s	-8.34	1.96				*b*
	5p	-5.24	1.90				
	4d	-10.50	4.54	(0.6097)	1.90	(0.6097)	
W	6s	-8.26	2.34				*b*
	6p	-5.17	2.31				
	5d	-10.40	4.98	(0.6683)	2.07	(0.5422)	
C	2s	-21.4	1.625				*b*
	2p	-11.4	1.625				
O	2s	-32.3	2.275				*b*
	2p	-14.8	2.275				
H	1s	-13.6	1.30				*c*
S	3s	-20.0	2.122				*d*
	3p	-11.0	1.827				
	3d	-8.0	1.500				
Cl	3s	-26.3	2.183				*b*
	3p	-14.2	1.733				
N	2s	-26.00	1.95				
	2p	-18.60	1.95				*b*
P	3s	-18.6	1.75				*b*
	3p	-14.0	1.30				

[a] C_1 and C_2 are coefficients in a double-ξ expansion. [b] R. H. Summerville, R. Hoffmann, *J. Am. Chem. Soc.*, **98**, 7240 (1976). [c] R. Rein, N. Fukuka, H. Win, G. A. Clarke and F. E. Haris, *J. Chem. Phys.*, **45**, 4773 (1966). [d] M. M. L. Chen, R. Hoffmann, *J. Am. Chem. Soc.*, **98**, 1647 (1976).

From this result, it may be said that the geometrical preference to the ferrole complex is attributable to the stability of three orbitals.

Acknowledgement. This work was supported by a Grant-in-Aid for Free Research Project from the ministry of Education, Korea. The authors are very grateful to professor Myung-Hwan Whangbo at North Carolina State University for his discussion.

Appendex

The geometry for $W_2(NH_2)_4Cl_4(\mu\text{-}Cl)_2$ was taken from the experimental structue of $W_2(Py)_4Cl_4(\mu\text{-}Cl)_2$. Bond lengths and angles for calculations involving $W_2(SH)_4(OH)_4(\mu\text{-}S)_2$, $Ta_2(PH_3)_4Cl_4(\mu\text{-}H)_2$, and $Mo_2(OH)_6(NH_2)(C_4H_4)$ were taken from the experimental structure. The extended Hückel calculation[21] were carried out using modified Wolfsberg-Helmholz formula withe parameters listed in Table 1.

References

1. (a) J. H. Wengrovius, R. R. Schrock and C. S. Day, *Inorg. Chem.*, **20**, 1844 (1981); (b) K. Wieghardt, M. Hahn, W. Swiridoff and J. Weiss, *Inorg. Chem.*, **23**, 94 (1984); (c) M. T. Flood, R. F. Ziolo, J. E. Earley and H. B. Gray, *Inorg. Chem.*, **12**, 2153 (1973).
2. F. A. Cotton, *Polyhedron*, **4**, 667 (1987).
3. A. J. Scioly, M. L. Luetkens, R. B. Wilson, J. C. Huffman and A. P. Sattelberger, *Polyhedron*, **4**, 741 (1987).
4. J. Ko, *Bull. Kor. Chem. Soc.*, **9**, 121 (1988).

5. R. B. Jackson and W. E. Streib, *Inorg. Chem.*, **10**, 1760 (1971).
6. A. Bino, F. A. Cotton, Z. Dori and J. C. Sekutowski, *Inorg. Chem.*, **17**, 2946 (1978).
7. A. P. Sattelberger, R. B. Wilson and J. C. Huffman, *Inorg. Chem.*, **21**, 2392 (1982).
8. A. R. Chakravorty, F. A. Cotton, M. P. Diebold, D. B. Lewis and W. J. Roth, *J. Am. Chem. Soc.*, **108**, 971 (1986).
9. K. R. Dunbar, D. Powell and R. A. Walton, *Chem. Commun.*, 114 (1985).
10. L. B. Anderson, F. A. Cotton, D. Demarco, A. Fang, W. H. Ilsley, B. W. S. Kolthammer and R. A. Walton, *J. Am. Chem. Soc.*, **103**, 5078 (1981).
11. F. A. Cotton, L. R. Falvello, M. F. Fredrich, D. MeMarco and R.A. Walton, *J. Am. Chem. Soc.*, **105**, 3088 (1983).
12. M. H. Chisholm, D. M. Haffman and J. C. Huffman, *Organometallis*, **4**, 986 (1985).
13. M. P. Brown, A. N. Keith, Lj Manojlovic-Muir, K. W. Muir, R. J. Puddephatt, K. P. Seddon *Inorg. Chem. Acta*, **34**, 1223 (1979).
14. D. M. Hoffman and R. Hoffmann, *Inorg. Chem.*, **20**, 3543 (1981),
15. A. J. Benton, M. G. B. Brew, R. J. Hobson and D. A. Rice, *J. Chem. Soc., Dalton Trans.*, 1304 (1981).
16. M. G. B. Drew, D. A. Rice and D. M. William, *J. Chem. Soc., Dalton Trans.*, 417 (1985).
17. G. C. Campbell, J. M. Canich, F. A. Cotton, S. A. Duraj and J. F. Haw, *Inorg. Chem.*, **25**, 287 (1986).
18. F. A. Cotton, M. P. Diebold, C. J. O. Connor and G. L. Powell, *J. Am. Chem. Soc.*, **107**, 7438 (1985).
19. M. H. Chisholm, K. Folting, J. C. Huffman, I. P. Rothwell, *J. Am. Chem. Soc.*, **104**, 4389 (1982).
20. D. L. Thorn and R. Hoffmann, *Inorg. Chem.*, **17**, 126 (1978).
21. R. Hoffman, W. N. Lipscomb, *J. Chem. Phys.*, **36**, 2179 (1962).

New Crown Compounds Derived from 1,2-Bis(2-hydroxybenzyl)benzene(I)

Woo Young Lee*, Chang Hee Park, Sung-Hwan Bang, Sang Goo Lee, and Wonbo Sim

Department of Chemistry, Seoul National University, Seoul 151-742. *Received July 13, 1989*

By cyclocondensation of 1,2-bis(2-hydroxybenzyl)benzene with oligoethylene glycol ditosylate, new crown ethers containing 1,2-dibenzylbenzene subunit were synthesized. By oxidation of the benzylic positions of them, carbonyl-containing crowns having 1,2-dibenzoylbenzene subunit were synthesized.

Introduction

Among various macrocyclic polyethers, many of them have aromatic hydrocarbon groups to which ethyleneoxy units are linked as the basic repeating structure, because they have been synthesized in general from di- or polyhydroxy aromatic compounds. For example, the benzocrown I[1-3], synthesized by C. J. Pedersen in his early work of crown ether synthesis, is a corand[4] in which ethyleneoxy chain is separated by two carbon atoms in the *o*-phenylene group. In naphthaleno-crown II[5], the ethyleneoxy chain is separated by three carbon atoms in the naphthene unit. The biphenyl crown III[3,6], prepared by D. J. Cram *et al.*, is another corand in which ethyleneoxy chain is separated by four carbon atoms in the biphenyl moiety. These three corands have similarities in structural constitution and properties, though they contain different hydrocarbon units.

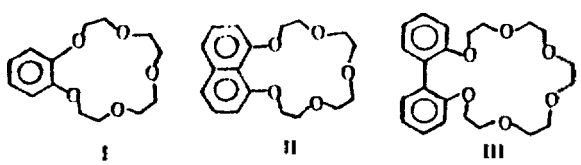

I II III

Now, we wish to report new crown ethers which are structurally related with the corands I-III, but in which ethyleneoxy chains are separated by eight carbon atoms in the aromatic hydrocarbon subunit. In this work, we also report novel crowns possessing ketonic carbonyl group as part of the macroring. We have been interested for many years in the synthesis of carbonyl crowns in which ether oxygens are substituted partially or completely for carbonyl groups, and this is one of the series of the investigation.

Results and Discussion

New crown ethers IV were synthesized by the condensation of 1,2-bis(2-hydroxybenzyl)benzene with oligoethylene glycol ditosylate in the presence of base. In this reaction, a small amount of side products were produced as well, which were known to be a symmetrical crown ethers having two or more 1,2-dibenzylbenzene subunits bound by ethyleneoxy units. The new corands IV are structurally related with the corands I-III, but IV are more flexible in a conformational sense, because the hydrocarbon unit in IV is flexible, wheras those in II and III are rigid. The molecular model shows that three benzene rings in IV are not neccessarily in a plane, but properly arranged rotating about the benzylic carbon between benzene rings to form a bent structue, which makes